Article | Received 13 June 2025; Revised 19 September 2025; Accepted 9 October 2025; Published 29 October 2025
https://doi.org/10.55092/asymmetry20250006

Recognition of the interiors of de Sitter-Kerr black holes from their shadows

Irina Dymnikova

A.F. Ioffe Physico-Technical Institute, St. Petersburg 194021, Russia; E-mail: igd.ammp@mail.ioffe.ru.

Highlights:

- Shadow of de Sitter-Kerr black hole.
- Relation of its mass function with celestial coordinates of its shadow.

Abstract: We investigate the asymmetry of shadows of rotating black holes, as a source of information on their interior content, for black holes of the Kerr-Schild class, specified by $T_t^t = T_r^r$. Non-singular black holes of the Kerr-Schild class, satisfying the weak energy condition, are described by de Sitter-Kerr solutions, asymptotically de Sitter as $r \to 0$. We obtain the direct relation between the mass function for a de Sitter-Kerr black hole, and the celestial coordinates of its shadow, as well as the direct relation of the interior density for an extreme black hole with the celestial coordinates of its double horizon, which presents the boundary of its shadow. Application of these relations for analysis of an observed black hole shadow would allow to get information on its interior content, and to consider the presence or absence+ of a singularity in its deep interior.

Keywords: black hole shadow; de Sitter-Kerr black hole; mass function; relation of mass function with celestial coordinates

1. Introduction

Information on a rotating black hole interior can be extracted in principle from the results of the direct observation of its shadow, seen by a distant observer as a dark region within the image of a bright source of radiation situated behind the black hole. The shape of a black hole shadow is determined by the photons gravitational capture cross-section, bounded by the innermost closed photon orbits [1–4].

Photon geodesics required for analysis of black hole shadows have been studied for the Kerr metric in [1–5], and later on for the Kerr-like metrics in [6–10]. General analysis and classification of the equatorial photon orbits in the field of non-singular rotating black holes of the Kerr-Schild class have been presented in our paper [11], including the detailed analysis of the innermost photon orbits with the special attention to the general characteristic properties and location of light rings, formed by the closed photon orbits.

Copyright©2025 by the authors. Published by ELSP. This work is licensed under a Creative Commons Attribution 4.0 International License, which permits unrestricted use, distribution, and reproduction in any medium provided the original work is properly cited.

In the paper [9] the critical curve has been introduced, which provides the precise distinction and informative description of the shadow boundary as presented by a photon ring, accumulating photons on the innermost orbits including photons winding for some time around a black hole before escaping to a distant observer, where they form, on his image plane, a bright photon ring confining the black hole shadow by the critical curve. Photons, that make only a fraction of an orbit, would generically contribute to a much wider lensing ring with the width about $(0.5 \div 1)\, M,$ which is centered at a radius 5% larger than the photon ring, can be relatively brighter by a factor of $2 \div 3$ and provide a significant observational signature in high resolution images [9]. The photon ring structure was investigated in the paper [12] for several spherically symmetric black hole metrics. An impact of an accretion disk on the shadow shape has been studied in the paper [13]. It was shown that physical effect of the accretion disk makes it difficult to obtain the clear observational distinction between the Kerr black hole and other compact objects. Analysis of Several spherically symmetric black hole and wormhole models, characterized by the existence of a second critical curve, revealed, for the case of thin accretion disks, appearance of additional photon rings between two critical curves. Observation of such rings would suggest the existence of compact objects able to mimick the black hole behavior [13]. The question of existence of compact objects without the event horizon, able to produce the shadows similar to those for black holes, has been addressed also in the paper [14]. Detailed analysis of shadow curves has shown the existence of several differences between the shadows of black holes and of other compact objects [14].

Theoretical analysis of the image of a rotating compact object, illuminated by a geometrically and optically thin disk on the equatorial plane, was presented in the paper [15]. Authors reported the existence of a new phenomenon which is the disruption and even disappearance of the photon ring dependently on the observational angle.

Question of deviations from the Kerr geometry was addressed on general setting in the paper [16], where approximate expressions have been obtained for the diameters, displacements, and asymmetries of photon rings around the Kerr and Kerr-like black holes. In this paper a new Kerr-like metric has been also presented; detailed calculation of the semi-analytic expressions for the shape of photon ring in this metric revealed its high asymmetry level [16].

The paper [17] has been devoted to study of the interferometric signature of a shadow image presented by a bright, narrow curve in the sky and its projected position function, measured in the interferometric observations. Authors have shown that this signature can be entirely reconstructed from its projected position confirming the ability of space interferometry to determine the shape of the photon ring. Analysis of the Kerr critical curve in this framework allowed to obtain its form in more details [17].

In the paper [18] a precise test of General Relativity in the strong field regime was proposed based on the detailed determination of the shape of the black hole photon ring. It was shown that the photon ring around the Kerr black hole provides the direct probe of the unstable bound photon orbits in the Kerr geometry, emphasizing that the precise shape of the photon ring is highly insensitive to the nature of an astrophysical source illuminating the black hole [18].

The effect of deviations from the Kerr metric on the photon rings has been investigated in the paper [19] in the framework of the photon ring-test of the Kerr hypothesis, based on the results, established in [18], that the GR-predicted shape of photon rings is insensitive to the details of the astrophysical source and can be measured by the space interferometry. Authors used the ray tracing code Gyoto for simulation of images of the Kerr black hole with thin equatorial accretion disk, repeating analysis for hundreds of models with different source profiles, black hole spins, and observer inclinations. The result allowed to describe how the width of the photon ring varies with different models [19].

In the paper [20] the influence of deviations from the Kerr metric on the black hole image has been studied in the framework of General Relativistic Radiation Transport simulations for a Kerr-Like metric with four free nonlinear deviation functions, applying the RAPTOR I code for generating the images. Analysis of the asymmetry, diameter, and shadow location in comparison with those for the Kerr metric has shown that such deviations exert strong influence on the shadow shape [20].

In the paper [21] authors have considered deviations on the Kerr metric, which involve additional parameters modifying the multipole structure of the Kerr geometry, in the framework of gravitational wave observations of the post-merger ringdown signal from black hole binaries. Bayesian analysis, using current and future gravitational wave data, has shown that involving higher modes, available for observations with future detectors, would allow to constrain deviations from the Kerr quadrupole mode on the percent level [21].

Possibilities of getting information on the basic characteristics of a black hole from observations of its shadow have been investigated in papers [22,23], devoted to measurement of the spin, and in the paper [24], devoted to testing the geometry of black hole candidates with using the data of radio and X-ray observations. Sensitivity of the obtained information to the position and motion of an observer with respect to the black hole has been investigated in [25,26].

The Kerr black hole is described by the metric (written in the geometrical units $c = G = 1$).

$$ds^2 = \frac{2Mr - \Sigma}{\Sigma}dt^2 + \frac{\Sigma}{\Delta}dr^2 + \Sigma d\theta^2 - \frac{4aMr\sin^2\theta}{\Sigma}dtd\phi + \left(r^2 + a^2 + \frac{2Mra^2\sin^2\theta}{\Sigma}\right)\sin^2\theta d\phi^2, \quad (1)$$

$$\Sigma = r^2 + a^2\cos^2\theta; \;\; \Delta = r^2 - 2Mr + a^2. \quad (2)$$

The parameter M is interpreted as the mass of a black hole and the parameter a is identified as its angular momentum [27]. Dependence of the shadow shape for the Kerr black on its angular momentum and orientation with respect to an observer, has been studied in [4,22,23,28,29].

The Kerr metric (1) can be obtained from the Schwarzschild metric by the complex coordinate transformation discovered by Newman and Janis in 1965 [30] $(r,t) \to (r,u)$; $u = t - \int \frac{dr}{g(r)}$; $r \to r + ia\cos\theta$; $u \to u = ia\cos\theta$.

In 1975 Gürses and Gürsey [31] have shown that this transformation works for metrics

$$ds^2 = g(r)dt^2 - \frac{dr^2}{g(r)} - r^2 d\Omega^2; \;\; g(r) = 1 - \frac{2\mathscr{M}(r)}{r}; \;\; \mathscr{M}(r) = 4\pi\int_0^r \tilde{\rho}(x)x^2 dx \quad (3)$$

which belong to the Kerr-Schild class of algebraically special solutions [32] to the Einstein equations, generated by source terms with the algebraic structure [33]

$$T_t^t = T_r^r. \quad (4)$$

Non-singular spherically symmetric solutions of the Kerr-Schild class, satisfying the weak energy condition [34], which requires non-negativity of density on any time-like curve, have the de Sitter center, $r = 0$, where the stress-energy tensor takes the maximally symmetric form $T_k^i = \rho\delta_k^i$, corresponding to the de Sitter vacuum with $p=-\rho$ [35]. Reducing its symmetry to the radial Lorentz boosts (4) leads to intrinsic anisotropy of pressure: $p_r=-\rho;\ \ p_\perp=-\rho-r\rho'/2$, where $\rho=T^t_t,\ \ p_r=-T^r_r,\ \ p_\perp=-T^\theta_\theta=-T^\phi_\phi$ [33,35].

The most of presented in the literature axially symmetric solutions for rotating objects belong to the Kerr-Schild class, and have been obtained with using the Newman-Janis algorithm [30], including the non-singular solutions [23,36,37]. Basic generic features of non-singular rotating black holes of this class have been studied in [38] (for a review [39]).

General formalism for transformation of spherically symmetric solutions of the Kerr-Schild class to axially symmetric solutions has been developed by Gürses and Gürsey on the basis of the complex Trautman-Newman translations, which include the Newman-Janis transformation. In the Boyer-Lindquist coordinates, related to the Cartesian coordinates x,y,z by $x^2+y^2=(r^2+a^2)\sin^2\theta;\ \ z=r\cos\theta$, the axially symmetric metrics have the form (written in the geometrical units $c=G=1$) [31]

$$ds^2=\frac{2f-\Sigma}{\Sigma}dt^2+\frac{\Sigma}{\Delta}dr^2+\Sigma d\theta^2-\frac{4af\sin^2\theta}{\Sigma}dtd\phi+\left(r^2+a^2+\frac{2fa^2\sin^2\theta}{\Sigma}\right)\sin^2\theta d\phi^2 \tag{5}$$

where the Lorentz signature is $[-\ +\ +\ +]$, and

$$\Delta=r^2+a^2-2f(r);\ f(r)=r\mathcal{M}(r);\ \Sigma=r^2+a^2\cos^2\theta. \tag{6}$$

In the axially symmetric spacetime the surfaces $r=const$ are the confocal ellipsoids [3]

$$r^4-(x^2+y^2+z^2-a^2)r^2-a^2z^2=0. \tag{7}$$

For $r=0$ the ellipsoids reduce to the equatorial disk

$$x^2+y^2\le a^2,\ \ z=0 \tag{8}$$

confined by the ring

$$x^2+y^2=a^2,\ \ z=0. \tag{9}$$

For the Kerr black hole (1) the ring (9) comprises its singularity. For non-singular black holes of the Kerr-Schild class, satisfying the weak energy condition, the master function in Equation (6) takes the form $f(r)=r^4/\,2r_0^2;\ \ r_0^2=3/8\pi\tilde{\rho}(0)$, the metric (5) coincides with the de Sitter metric in the co-rotating frame, and the de Sitter center of the original spherical solution becomes the equatorial de Sitter disk filled with the de Sitter vacuum together with the ring (9) [38]. For $r\to\infty$ the master function $f(r)$ tends to $f(r)=Mr$, and the metric (5) coincides with the Kerr metric (1). The mass of an object $M=4\pi\int_0^\infty\rho(r)r^2dr$, which appears as the mass parameter in the Kerr limit $r\to\infty$, is intrinsically related to the interior de Sitter vacuum and breaking of spacetime symmetry from the de Sitter group in the origin [35]. The dimensionless parameter which characterizes the de Sitter-Kerr black holes is $x_g=r_g/r_0$ where $r_g=2GM$.

The number of horizons in the de Sitter-Kerr spacetime depends on the generic behavior of the function $\Delta(r,a)$ in Equation (6), studied in detail in [38]; it was shown that de Sitter-Kerr spacetime can have at most two horizons, defined by $\Delta(r_+,r_-)=0$, which gives

$$r_{+,-}=\mathcal{M}(r)\pm\sqrt{\mathcal{M}^2-a^2} \tag{10}$$

where r_+ is the event horizon and $r_-<r_-$ is the internal Cauchy horizon. For the extreme black hole

with $a = a_{dh} = \mathscr{M}(r_\pm)$ the double horizon is definedd as $r_\pm = \mathscr{M}(r_\pm)$ [38]. The mass function for two particular de Sitter-Kerr solutions are presented below in Equations (11) and (12).

Now black hole shadows are available for the direct astronomical observations [28,40] due to the results presented by the Event Horizon Telescope Collaboration [41] on the first observation of the black hole shadow in M87 [42] and the first observation of the shadow of the supermassive black hole in the center of the Milky Way [43–46] (for a recent review [47]).

The first results on the black hole shadow for M87* adopted a distance to the object as (16.8 ± 0.8) Mpc, and evaluated a shadow diameter as (42 ± 3) $as(microarcseconds)$ and the black hole mass as $M = (6.5 \pm 0.7) \cdot 10^9\ M_\odot$, and the deviation from circularity as $\Delta C < 0.1$. For the supermassive black hole at the center of our galaxy, Sagittarius A*, EHT collaboration reported the diameter of (51.8 ± 2.3) as (with 68% credible interval), the mass of the black hole $M = (4.3 \pm 0.4) \cdot 10^6\ M_\odot$ ([47] and references therein).

The question of investigation of the black holes structure by analysis of data on observations of their shadows has been considered in [48] for super-spinning black holes violating the Kerr bound, which constrains the specific angular momentum of a black hole by its mass in the geometrical units and whose violation suggests the existence of super-spinning objects [49], as well as in the framework of the $\delta = 2$ Tomimatsu-Sato solution [50], and of testing the no-hair theorem with the observations data depending on a black hole quadrupole moment [51]. The results similar to those for the Kerr black hole have been obtained for analysis of the non-Kerr black holes [23], in the framework of different gravity theories [52], for black hole images obtained from the general relativistic transfer [53], for hydrodynamical simulations of black hole accretion [54] with using the Rezzola-Zhidenko parametrization in general metric theories [55], and for a dilaton black hole in the Einstein-Maxwell-axion gravity [56] (for a recent review [57]).

In our paper [58] we have presented the general description of shadows for black holes of the Kerr-Schild class, and have shown that shadows of the de Sitter-Kerr black holes are less than the shadow of the Kerr black hole, and that the asymmetry of their shadows increases with increasing the angular momentum of the black hole, as for the Kerr black hole, but in addition the asymmetry of the de Sitter-Kerr shadows strongly depends on the pace of decreasing of the interior density [58]. We have compared shadows of two de Sitter-Kerr black holes with the shadow of the Kerr black hole of the same mass. The first is described by the regular axially symmetric solution obtained from the spherical solution with the quickly decreasing density profile and the mass function given by [33]

$$\tilde{\rho}(r) = \rho_0 e^{-r^3/r_s^3}; \quad \mathscr{M}(r) = M(1 - e^{-r^3/r_s^3}); \;\; r_s = (r_0^2 r_g)^{1/3}. \tag{11}$$

It was adopted for description of the vacuum polarization by the gravitational field in the semiclassical model, based on the hypothesis on symmetry restoration at in the course of the gravitational collapse, when all fields contribute to vacuum polarization and thus to gravity via the Einstein equations [33,35].

The parameter $r_s = (r_0^2 r_g)^{1/3}$, appeared in the non-singular solution, represents the length scale characteristic for spacetime structures with the de Sitter interiors [33,59].

The second axial solution is obtained with the slowly decreasing phenomenologically regularized Newtonian profile and the mass function given by [38]

$$\tilde{\rho} = \frac{\tilde{\rho}_0^2}{(r^2/r_v^2+1)^2}; \quad \mathscr{M}(r) = \frac{2M}{\pi}\left[\arctan\frac{r}{r_v} - \frac{rr_v}{r^2+r_v^2}\right]; \quad r_v = \left(\frac{4r_0^2 r_g}{3\pi}\right)^{1/3} = \left(\frac{4}{3\pi}\right)^{1/3} r_s. \tag{12}$$

The regularization parameter r_v corresponds to the length scale, defined by the strong energy condition, $\tilde{\rho} + \sum_k \tilde{p}_k \geq 0$, responsible for non-negativity of the gravitational acceleration in the singularity theorems [34]. The length scale r_v determines the surface of zero gravity, beyond which the strong energy condition is violated and the gravitational attraction is changed by the gravitational repulsion, $\tilde{\rho} + \sum_k \tilde{p}_k = 0 \rightarrow \tilde{\rho}_0 r_v^4 (r^2 - r_v^2)/(r^2 + r_v^2)^3 = 0$.

In Figures 1–2 [58] the shadows of these two de Sitter-Kerr black holes are compared with the Kerr shadow, plotted by the dashed line, for two values of the angular moment $a = 0.7$ (Figure 1) and $a = 0.3$ (Figure 2). In Figure 1 (Left) and Figure 2 (Left) the shadow of the de Sitter-Kerr black hole with the quickly decreasing density (11) is compared with the shadow of the Kerr black hole of the same mass. In Figure 1 (Right) and in Figure 2 (Right) the shadow of the de Sitter-Kerr black hole with the slowly decreasing density (12) is compared with the shadow of the Kerr black hole. The basic parameter of the de Sitter-Kerr geometry $x_g = r_g/r_0$ is chosen as $x_g = 20.06$. The angular coordinate of an observer at infinity is $\theta_i = \pi/2$.

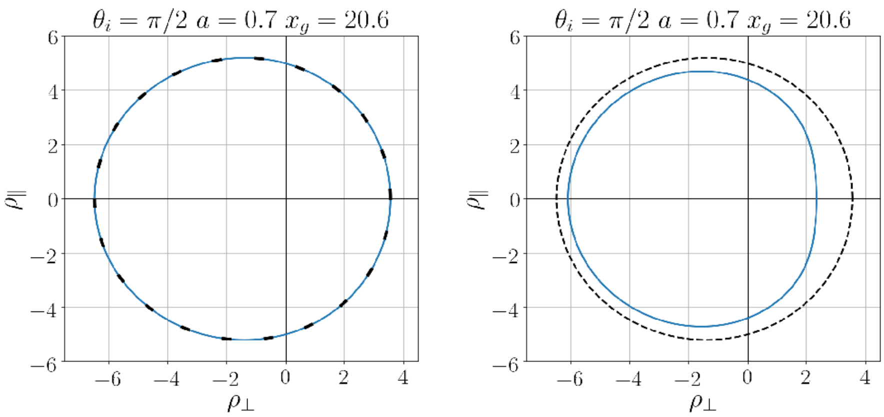

Figure 1. Comparison of shadows for the quickly decreasing density (11) **(Left)** and for the slowly decreasing density (12) **(Right)** for $a = 0.7$.

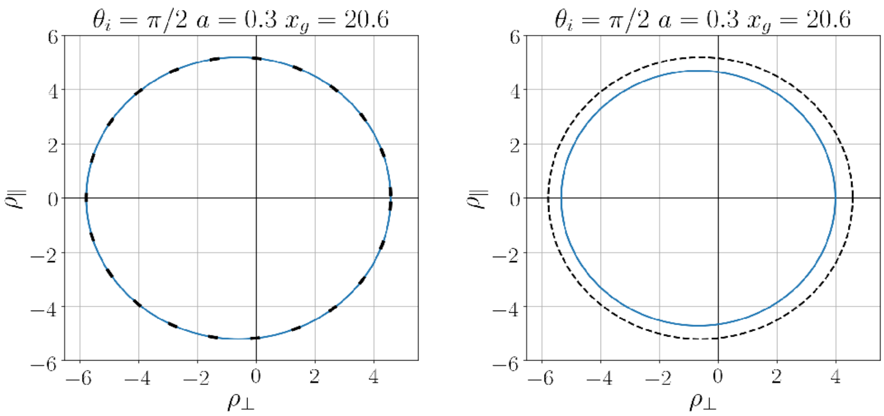

Figure 2. Comparison of shadows of the quickly decreasing **(Left)** and slowly decreasing **(Right)** density profiles for $a = 0.3$.

These pictures reveal the remarkable dependence of the de Sitter-Kerr black hole shadow on its interior density. The difference of the de Sitter-Kerr shadow from the Kerr shadow is essentially more significant for the slowly decreasing density profile (12) (Figure 1 (Right)) [58] than for a quickly falling density (11) when the de Sitter-Kerr shadow almost coincides with the Kerr shadow (Figure 1 (Left)) [58]. The assymmetry of shadow, exposed for the black hole with slowly decreasing density profile, decreases with decreasing the angular momentum as we see comparing Figure 1 (Right) with Figure 2 (Right).

Our aim in this paper is to obtain the direct relation between the mass function and the interior density for de Sitter-Kerr black holes and the celestial coordinates of their shadows, which would allow to get information about the character of the black hole interiors from the analysis of their shadows.

In Section 2 we introduce the basic equations which describe the behavior of photons responsible for the formation of the boundary of the black hole shadow. In Section 3 we derive the relation between the celestial coordinates of the black hole shadow and its mass function and the interior density. Section 4 contains conclusions.

2. Description of the black hole shadow

The shape of the black hole shadow corresponds to the gravitational capture cross-section, confined by the innermost closed photon orbits [3].

In the axially symmetric geometry spacetime symmetry is characterized by the Killing vectors K_t and K_ϕ, responsible for the existence of the integrals of motion E and L_z, respectively. In addition there exists also the conformal Killing tensor $K_{\alpha\beta}$, since the geometry (5) belongs to spacetimes of the D-type in the Petrov classification. This provides the existence of the quadratic integral of motion $\mathscr{K}^2$ and the related integral of motion Q, defined by ([3,4] and references therein)

$$\mathscr{K}^2 = Q + (L_z - aE)^2. \tag{13}$$

Normalization of the integral of motion L_z on E and of the integral Q on E^2 gives the integrals of motion in the dimensionless form, basic for description of the black hole shadows

$$\xi = L_z/E; \quad \eta = Q/E^2. \tag{14}$$

The general equations for the photon geodesics read [3]

$$\dot{r}^2 = \frac{E^2}{\Sigma^2}\mathscr{R}(r); \quad \mathscr{R}(r) = r^4 + (a^2 - \xi^2 - \eta)r^2 + [\eta + (\xi - a)^2]2\mathscr{M}(r)r - a^2\eta;$$

$$\dot{\theta}^2 = \frac{E^2}{\Sigma^2}\Theta(\theta); \;\; \Theta(\theta) = \eta + a^2\cos^2\theta - \xi^2\cot^2\theta;$$

$$\dot{\phi} = \frac{E}{\Sigma}\Phi(\phi);\; \Phi(\phi) = \frac{\xi^2}{\sin^2\theta} + \frac{a}{\Delta}[2\mathscr{M}(r)r - a\xi];\; \dot{t} = \frac{E}{\Sigma}\left(-a^2\sin^2\theta + \frac{1}{\Delta}[(r^2+a^2)^2 - 2a\mathscr{M}(r)r\xi]\right) \tag{15}$$

where the dot means the derivative with respect to the affine parameter on a geodesic.

The real positive root $r \geq r_+$ of the equation $\mathscr{R}(r) = 0$ defines the distance of the closest approach of a photon to the black hole as the turning point on the photon trajectory. The minimal distance determines the radius of the innermost closed photon orbit which contributes to the formation of the shadow contour. The equation for the turning point $\mathscr{R}(r) = 0$ reads [4]

$$(r^2 + a^2 - a\rho_\perp \sin\theta_i)^2 - \Delta\left[\rho_{||}^2 + (\rho_\perp - a\sin\theta_i)^2\right] = 0. \tag{16}$$

The impact parameters $\rho_\perp$ and ρ are determined by the integrals of motions as [3,4]

$$\rho_\perp = r^2 \sin^2\theta_i \left(\frac{d\phi}{dt}\right)_\infty = \frac{\xi}{\sin\theta_i}; \;\; \rho_{||} = r^2\left(\frac{d\theta}{dt}\right)_\infty = \pm\sqrt{\eta + a^2\cos^2\theta_i - \xi^2\cot^2\theta_i}. \tag{17}$$

The angle θ_i is the angle coordinate of an observer [3].

The impact parameters correspond to the celestial coordinates of the turning point as

$$x = \rho_\perp = \frac{\xi}{\sin\theta_i}; \;\; y = \rho_{||} = \pm\sqrt{\eta + a^2\cos^2\theta_i - \xi^2\cot^2\theta_i}. \tag{18}$$

The impact parameters are shown in Figure 3 (Left) [4,58], where $\rho = \sqrt{\rho_\perp^2 + \rho_{||}^2}$.

The celestial coordinate x presents the apparent distance of the black hole image from the symmetry axis perpendicular to it, while the coordinate y presents the apparent distance of the black hole image from its projection on the equatorial plane. In the case of the minimal closest approach of the photon they determine the celestial coordinates (x, y) of the shadow contour.

The asymmetry parameter D shown in Figure 3 (Right) [58] is introduced with using the fitting circle with the the radius $R = x_C - x_L$ and the center $x = x_C$, the coordinates of an upper point of the shadow boundary (x_t, y_t) and of its left and right endpoints in the equatorial plane x_L and x_R. The parameter D is the distance between the right endpoints of the circle and shadow contour $D = 2R - (x_R - x_L)$ [22]. With account for $R^2 = (x_C - x_t)^2 + y_t^2$ one can eliminate x_C, obtain $R = (y_t^2 + (x_t - x_L)^2)/(2(x_t - x_L))$ and introduce the distortion parameter in terms of the celestial coordinates [58] $\delta = D/R = 2[1 - (x_R - x_L)(x_t - x_L)/(y_t^2 + (x_t - x_L)^2)]$.

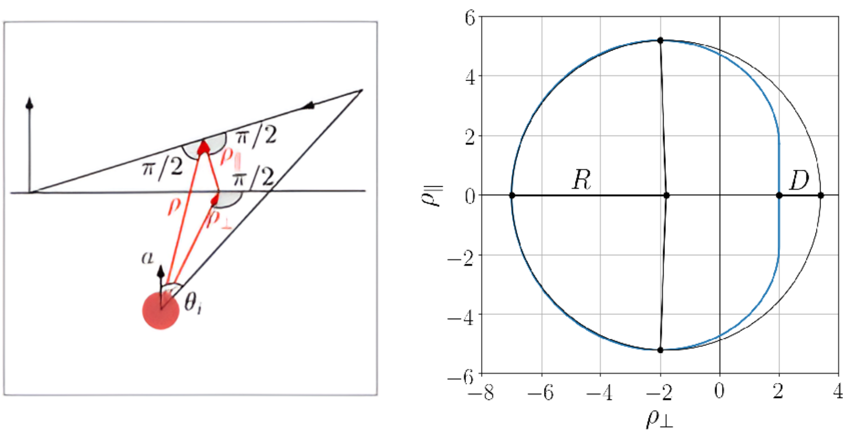

Figure 3. (Left) Impact parameters $\rho_\perp$ and $\rho_{||}$. **(Right)** Asymmetry parameter D.

In the next Section we derive the direct relation of the celestial coordinates for a de Sitter-Kerr black hole with its mass function and the interior density, which would allow ro extract information on the black hole interior content from analysis of shadow observations.

3. Recognition of the mass function and the density

The boundary of the shadow is formed by the innermost closed photon orbits $r = const$ which satisfy the equations [58]

$$\mathscr{R}(r) = 0; \;\; \partial\mathscr{R}/\partial r = 4r^3 + 2(a^2 - \xi^2 - \eta)r + 2(\mathscr{M} + \mathscr{M}'r)[\eta + (\xi - a)^2] = 0. \tag{19}$$

Solution to this system of two algebraic equations gives two integrals of motion ξ and η on the photon orbits, responsible for the shadow contour, as [58]

$$\xi = \frac{\mathscr{M}(r^2-a^2) - r\Delta - \mathscr{M}' r(r^2+a^2)}{a(r-\mathscr{M}-\mathscr{M}'r)}^2; \tag{20}$$

$$\eta = \frac{r^3}{a^2(r-\mathscr{M}-\mathscr{M}'r)}\left[4a^2\mathscr{M} - r(r-3\mathscr{M})^2 - 2\mathscr{M}'r(r^2-3\mathscr{M}r+2a^2) - (\mathscr{M}')^2 r^3\right]. \tag{21}$$

In the case $\mathscr{M} = M = const$ they coincide with the corresponding integrals of motions in the Kerr geometry (1) presented in [3].

Normalizing the integral $\mathscr{K}^2$ on E^2 and keeping its notation (13), we express it in terms of the integrals of motion ξ and η as

$$\mathscr{K}^2 = \eta^2 + (\xi - a)^2. \tag{22}$$

In the celestial coordinates (18) this yields

$$\mathscr{K}^2 = y^2 + (x - as)^2;\ s = \sin\theta_i. \tag{23}$$

Integrals of motion (20) and (21) can be presented via the function Δ and its derivative as

$$\xi = \frac{1}{a}\left[r^2 + a^2 - 4r\frac{\Delta}{\Delta'}\right]. \tag{24}$$

$$\Delta'\eta = 4r^3 - 4ra(\xi - a) - \Delta'(\xi - a)^2. \tag{25}$$

It follows

$$\eta = \frac{1}{a^2(\Delta')^2}\left[r^4(\Delta')^2 - \Delta'(3r^3a^2 + 8r^3\Delta) + 16r^2\Delta(\Delta + a^2)\right]. \tag{26}$$

Applying the Equations (24) and (26) in the Equation (22), we express the integrals of motion ξ and $\mathscr{K}^2$ as

$$\xi - a = \frac{1}{a}\left[r^2 - 4r\frac{\Delta}{\Delta'}\right];\quad \mathscr{K}^2 = \frac{16r^2\Delta}{(\Delta')^2}. \tag{27}$$

Introducing the variables

$$u = r^2;\ \ v = \sqrt{\Delta} \tag{28}$$

and taking into account Equation (27), we obtain the system of two equations for the variables u and v

$$u\frac{dv}{du} - v = \frac{a(\xi - a)}{\mathscr{K}};\quad \frac{dv}{du} = \frac{1}{\mathscr{K}}. \tag{29}$$

Using the Equations (18) and (23) we obtain the system (29) in the form involving the celestial coordinates

$$\frac{dv}{du} = \frac{1}{\sqrt{y^2 + (x-as)^2}};\quad u\frac{dv}{du} - v = \frac{a(xs-a)}{\sqrt{y^2 + (x+as)^2}}. \tag{30}$$

Differentiation of these equations with respect to u yields

$$u\frac{d^2v}{du^2} = \frac{dx}{du}\left[\frac{\partial}{\partial x} + \frac{dy}{dx}\frac{\partial}{\partial y}\right]\frac{a(xs-a)}{\sqrt{y^2+(x-as)^2}};$$

$$\frac{d^2v}{du^2} = \frac{dx}{du}\left[\frac{\partial}{\partial x} + \frac{dy}{dx}\frac{\partial}{\partial y}\right]\frac{1}{\sqrt{y^2+(x-as)^2}}. \tag{31}$$

From this system we find

$$u = \left(\left[\frac{\partial}{\partial x} + \frac{dy}{dx}\frac{\partial}{\partial y} \right] \frac{a(xs-a)}{\sqrt{y^2+(x-as)^2}} \right) \Big/ \left(\left[\frac{\partial}{\partial x} + \frac{dy}{dx}\frac{\partial}{\partial y} \right] \frac{1}{\sqrt{y^2+(x-as)^2}} \right). \tag{32}$$

After simple calculations we obtain the variable u in terms of the celestial coordinates

$$u = a(xs-a) - as\frac{y^2+(x-as)^2}{x-as+y\,dy/dx}. \tag{33}$$

Now the variable v can be found from the Equation (30) written in terms of the celestial coordinates, which gives

$$\frac{u}{\sqrt{y^2+(x+as)^2}} - v = \frac{a(xs-a)}{\sqrt{y^2+(x-as)^2}} \tag{34}$$

and hence,

$$v = \frac{u-a(xs-a)}{\sqrt{y^2+(x-as)^2}}. \tag{35}$$

Putting here u from Equation (33) we obtain the variable v as the function of the celestial coordinates

$$v = -as\frac{\sqrt{y^2+(x-as)^2}}{x-as+y\,dy/dx}. \tag{36}$$

and find from Equations (28), (33) and (36) that

$$\Delta = \frac{a^2s^2(y^2+(x-as)^2)}{(x-as+y\,dy/dx)^2} = r^2+a^2-2\mathscr{M}(r)r. \tag{37}$$

Finally, taking into account Equations (28) and (33) in the Equation (37), we obtain the direct relation between the mass function $\mathscr{M}(r)$ for a black hole and the celestial coordinates of its shadow

$$2r\mathscr{M}(r) = \left[\frac{as(y^2+(x-as)^2)}{(x-as+y\frac{dy}{dx})^2}\left(x+y\frac{dy}{dk}\right) - x \right]. \tag{38}$$

The relation of the celestial coordinates of the shadow with the radius of the photon orbits, which contribute to its boundary, follows from the Equation (16) written in the celestial coordinates (18), which gives

$$(r^2+a^2-axs)^2 - \Delta[y^2+(x-as)^2] = 0. \tag{39}$$

In the case when the celestial coordinates of the shadow are known, this equation gives the capture cross-section confined by the photon orbits, which form the shadow boundary.

As a result we have the system of two Equations (38) and (39) for two variables, the radius r of the photon orbit on the shadow contour and the mass function $\mathscr{M}(r)$ for this orbit.

Applying these equations for the observed shadow of a black hole with the known values of the parameters s and a, we get information about behavior of the mass function for this black hole. Taking the points (x,y) on the shadow contour and calculating the derivative dy/dx in these points, we can restore the function $\mathscr{M}(r)$ for the values of r, corresponding to the photon orbits, which determines the shadow contour.

Photon orbits are typically described by the equation $E^2 - V_\gamma(r) = 0$ where $V_\gamma(r) = (\xi^2-a^2)/r^2 - (2\mathscr{M}(r)/r^3)(\xi-a)^2$. For de Sitter-Kerr black holes the mass function vanishes at $r=0$ as $\mathscr{M}(r) \propto r^3$, and the potentials $V_\gamma(r)$ decrease from $V_\gamma(r) \to \infty$ at $r = 0$, which makes possible the existence of the innermost stable orbits in their minima.

The basic properties and sequence of circular equatorial photon orbits has been studied in our papers [11] by analysis of the orbit curve $r(a)$, shown below in Figure 4 (Left) [11], with the enhanced image of its fragment near the double horizon (Figure 4 (Right)) [11]. Ergosphere shown in Figure 4 is the surface of the static limit defined by $g_{tt} = 0$. It confines the ergoregion, where $g_{tt} < 0$, which enables the extraction of energy from a rotating black hole.

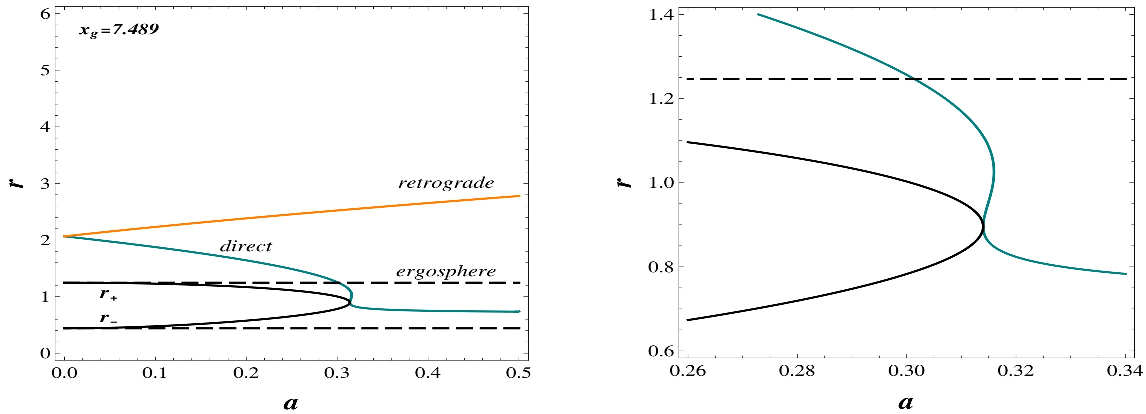

Figure 4. Radii of photon orbits, horizons and ergosphere dependently on a **(Left)** and their enhanced image near the double horizon **(Right)**; $x_g = r_g/r_0$.

For co-rotating orbits the curve $r(a)$ has two branching points, on the double horizon $r_\pm$ for $a = a_{dh}$, and at $r_{br\gamma} > r_\pm$ for $a_{br\gamma} > a_{dh}$. In the black hole region, $a \le a_{dh}$, there exist one branch of unstable retrograde orbits with $dr/da > 0$, and one branch of direct (co-rotating) orbits with $dr/da < 0$, stable or unstable dependently on the mass function [11].

For an extreme black hole the innermost photon orbit exists on the double horizon $r_- = r_+ = r_\pm = \mathscr{M}(r_\pm) = a_{dh}$ [11] and represents the boundary of its shadow.

Equations (27) and (23) for the integral of motion $\mathscr{K}$ give

$$\mathscr{K} = \sqrt{y^2 + (x - as)^2} = 4r\frac{\sqrt{\Delta}}{\Delta'}. \tag{40}$$

On the double horizon we have

$$\Delta = (r_\pm - \mathscr{M})^2; \;\; \Delta' = 2(r_\pm - \mathscr{M})(1 - \mathscr{M}'); \;\; \frac{\sqrt{\Delta}}{\Delta'} = \frac{1}{2(1 - \mathscr{M}')}. \tag{41}$$

In the dimensionless variables $r \to r/(GM)$, and the mass function, normalized to the mass parameter M, reads

$$\mathscr{M}(r) = \frac{3x_g^2}{8}\int_0^r \tilde{\rho}(z) z^2 dz; \;\; x_g = \frac{r_g}{r_0}; \;\; r_g = 2GM; \;\; r_0^2 = \frac{3}{8\pi G\tilde{\rho}_0} \tag{42}$$

where $\rho_0 = \rho(r = 0)$, and $\rho(r)$ is normalized to ρ_0. It follows that

$$\mathscr{M}'(r) = \frac{3x_g^2}{8}\rho(r)r^2. \tag{43}$$

On the double horizon the Equations (40) and (41) give

$$\mathscr{K} = \sqrt{y^2 + (x - as)^2} = \frac{2r}{1 - \mathscr{M}'} = \frac{2r}{1 - (3x_g^2/8)\rho(r)r^2}. \tag{44}$$

As a result we obtain the relation between the density on the double horizon and its celestial coordinates as

$$\frac{3x_g^2}{8}\rho(r)r^2 = 1 - \frac{2r}{\sqrt{y^2 + (x - as)^2}}. \tag{45}$$

According to the Equation (27), $a(xs - a) = [r^2 - 4r\Delta/\Delta']$. On the double horizon $\Delta/\Delta' = (r - \mathscr{M})^2/[(r - \mathscr{M})(1 - \mathscr{M}')] = 0$, and the Equation (27) gives $r_\pm^2 = a(xs - a)$. Then the Equation (45) yields the direct relation between the density on the double horizon of the extreme black hole and its celestial coordinates

$$\frac{3x_g^2}{8}\rho(r) = \frac{1}{a(xs - a)} - \frac{2}{\sqrt{a(xs - a)}\sqrt{y^2 + (x - as)^2}}. \tag{46}$$

On the other hand, we can evaluate the density from the restored mass function in Eqauation (38) which gives

$$\frac{d\mathscr{M}}{dr} = \frac{3x_g^2}{8}\rho(r)r^2. \tag{47}$$

If for a certain point r the density $\rho(r)$, obtained from the restored mass function $\mathscr{M}(r)$, coincides with the density (46), this suggests that the black hole is extreme. Then the relation (46) gives the value of the density on the double horizon $r_\pm$, which forms the boundary of its shadow. It is clear that, if the obtained value is non-zero, it means that we have not the Kerr black hole.

4. Conclusion

In this work we have studied the possibility to obtain information on the internal content of the rotating black holes from analysis of their shadows, for black holes, described by solutions of the Kerr-Schild class specified by $T_t^t = T_r^r$, to which belongs the most of solutions presented in the literature.

Geometry of rotating black holes of this class contains the equatorial disk $r = 0$ in their interiors. In the Kerr black hole the disk is confined by the ring singularity. For non-singular rotating black holes the interior disk $r = 0$ and the confining it ring comprise the de Sitter vacuum. For $r \to \infty$ their geometry asymptotically coincides with the Kerr geometry.

We have obtained the direct relation (38) between the mass function $\mathscr{M}(r)$ for de Sitter-Kerr black holes and the celestial coordinates of their shadows. The information on the mass function $\mathscr{M}(r)$ for a black hole comes from analysis of its shadow in a certain interval of the radius r for the photon orbits which form the boundary of the shadow. For this interval we can note a tendency in the behavior of the mass function $\mathscr{M}(r)$ dependently on r. For non-singular black holes, satisfying the weak energy condition, the mass function $\mathscr{M}(r)$ is monotonically increasing from zero to the mass parameter M at approaching the Kerr limit. If the restored mass function $\mathscr{M}(r)$ would appear non-zero and decreasing with decreasing r, this would testify that the black hole is non-singular. If the restored mass function would appear increasing with decreasing r, this suggests that the observed black hole can be singular. In the case when the relation (38) between the mass function $\mathscr{M}(r)$ and the celestial coordinates of its shadow gives zero values, this implies that we have the Kerr black hole.

For an extreme black hole we obtained the direct relation (46) between the density $\rho(r)$ on its double horizon, which presents the boundary of its shadow, and the celestial coordinates of this boundary. If for a certain value of the radius r the density $\rho(r)$, obtained from its relation (46) with the celestial coordinates of its double horizon, would coincide with the density $\rho(r)$, calculated from the restored mass function $\mathscr{M}(r)$, this suggests that the black hole is extreme. In this case the relation (46) between its density and the celestial coordinates of the boundary of its shadow, gives the direct information about the interior density $\rho(r)$ on the double horizon. If both restorations give zero values for the mass and for the density, we have the extreme Kerr black hole with the double horizon.

Summarizing we can suppose that an observed black hole belongs to the Kerr-Schild class (as the Kerr black hole) and satisfies the weak energy condition. We can then expect that using the relations, obtained in the Kerr-Schid framework, for analysis of data on the observed black hole shadow, would shed some light on its interior content and would allow to consider the presence/absence of a singularity in its deep interior. We plan our further research in this direction.

Conflicts of interests

The author declares no conflict of interest.

References

[1] Bardeen JM. Timelike and null geodesics in the Kerr metric. In *Black Holes (Les Astres Occlus)*. New York: Gordon and Breach Science Publishers, Inc., 1973. pp. 215–239.

[2] Young PJ. Capture of particles from plunge orbits by a black hole. *Phys. Rev. D* 1976, 14(12):3281–3289.

[3] Chandrasekhar S. *The mathematical theory of black holes*. Oxford: Clarendon Press, 1983.

[4] Dymnikova I. Motion of particles and photons in the gravitational field of a rotating body. *Sov. Phys. Usp.* 1986, 29(3):215–237.

[5] Teo E. Spherical photon orbits around a Kerr black hole. *Gen. Relativ. Gravitation* 2003, 35(11):1909–1926.

[6] Johannsen T. Photon rings around Kerr and Kerr-like black holes. *Astrophys. J.* 2013, 777(2):170.

[7] Yang X, Wang J. YNOGK: a new public code for calculating null geodesics in the Kerr spacetime 2012. *Astrophys. J. Suppl. Ser.* 2013, 207(1):6.

[8] Chan CK, Psaltis D, Oezel F. Photon rings around Kerr and Kerr-like black holes. *Astrophys. J.* 2013, 777:170.

[9] Gralla SE, Holz DE, Wald RM. Black hole shadows, photon rings, and lensing rings. *Phys. Rev. D* 2019, 100(2):024018.

[10] Teo E. Spherical orbits around a Kerr black hole. *Gen. Rel. Grav.* 2021, 53(1):10.

[11] Dymnikova I, Dobosz A, Sołtysek B. Classification of circular equatorial orbits around regular rotating black holes and solitons with the de Sitter/Phantom interiors. *Universe* 2022, 8(2):65.

[12] Wielgus M. Photon rings of spherically symmetric black holes and robust tests of non-Kerr metrics. *Phys. Rev. D* 2021, 104(12):124058.

[13] Guerrero M, Olmo GJ, Rubiera-Garcia D, Gómez DSC. Light ring images of double photon spheres in black hole and wormhole space-times. *Phys. Rev. D* 2022, 105(8):084057.

[14] Wang X, Hou Y, Guo M. How different are shadows of compact objects with and without horizons? *J. Cosmol. Astropart. Phys.* 2023, 2023(5):036.

[15] Wang X, Wang X, Zhang H, Guo M. Is a photon ring invariably a closed structure? *Eur. Phys. J. C* 2024, 84(11):1168.

[16] Johannsen T. Photon rings around Kerr and Kerr-like black holes. *Astrophys. J.* 2013, 777(2):170.

[17] Gralla SE, Lupsasca A. Observable shape of black hole photon rings. *Phys. Rev. D* 2020, 102(12):124003.

[18] Gralla SE, Lupsasca A, Marrone DP. The shape of the black hole photon ring: a precise test of strong-field general relativity. *Phys. Rev. D* 2020, 102(12):124004.

[19] Paugnat H, Lupsasca A, Vincent FH, Wielgus M. Photon ring test of the Kerr hypothesis: variation in the ring shape. *Astron. Astrophys.* 2022, 668:A11.

[20] Agurto-Sepulveda F, Lagunas JH, Pedreros J, Bandyopadhyay B, Schleicher DR. Exploring how deviations from the Kerr metric can affect SMBH images. *arXiv* 2023, arXiv:2309.11280.

[21] Dey K, Barausse E, Basak S. Measuring deviations from the Kerr geometry with black hole ringdown. *Phys. Rev. D* 2023, 108(2):024064.

[22] Hioki K, Maeda R. Measurement of the Kerr spin parameter by observation of a compact object's shadow. *Phys. Rev. D* 2009, 80(2):024042.

[23] Li E, Bambi C. Measuring the Kerr spin parameter of regular black holes from their shadow. *J. Cosmol. Astropart. Phys.* 2014, 2014(1):041–061.

[24] Bambi C. Testing the space-time geometry around black hole candidates with the available radio and X-ray data. *arXiv* 2013, arXiv:1301.0361.

[25] Grenzebach A. Aberration effects for shadows of black holes. *arXiv* 2015, arXiv:1502.02861.

[26] Mars K, Paganini CF, Oancea MA. The fingerprints of black holes—shadows and their degeneracies. *Classical Quantum Gravity* 2017, 35(2):025005.

[27] Carter B. Global structure of the Kerr family of gravitational fields. *Phys. Rev.* 1968, 174(5):1559–1571.

[28] Takahashi R. Shapes and positions of black hole shadows in accretion disks and spin parameters of black holes. *Astrophys. J.* 2004, 611(2):996–1004.

[29] Repin SV, Kompaneets DA, Novikov ID, Mityagina VA. Shadow of rotating black holes on a standard background screen. *arXiv* 2018, arXiv:1802.04667.

[30] Newman CT, Janis AJ. Note on the Kerr spinning particle metric. *J. Math. Phys.* 1965, 6(6):915–917.

[31] Gürses M, Gürsey F. Lorentz covariant treatment of the Kerr-Schild geometry. *J. Math. Phys.* 1975, 16(12):2385–2391.

[32] Kerr RP, Schild A. Some algebraically degenerate solutions of Einstein's gravitational field equations. In *Proceedings of Symposia in Applied Mathematics*, 1965, p. 199.

[33] Dymnikova I. Vacuum nonsingular black hole. *Gen. Rel. Grav.* 1992, 24(2):235–242.

[34] Hawking SW, Ellis GFR. *The Large Scale Structure of Space-Time.* Cambridge: Cambridge University Press, 1973.

[35] Dymnikova I. The cosmological term as a source of mass. *Classical Quantum Gravity* 2002, 19(4):725–740.

[36] Ayon-Beato A, Garcia A. The Bardeen model as a nonlinear magnetic monopole. *Phys. Lett. B* 2000, 493(1–2):149–152.

[37] Hayward SA. Formation and evaporation of regular black holes. In *7th International Conference on Gravitation and Cosmology*, Goa, India, December 14–19, 2011, pp. 1181–1183.

[38] Dymnikova I, Galaktionov E. Regular rotating de Sitter-Kerr black holes and solitons. *Classical Quantum Gravity* 2016, 33(14):145010.

[39] Dymnikova I. Regular rotating black holes and solitons with the de Sitter/Phantom interiors. In *Springer Series in Astrophysics and Cosmology (SSAC)*, 1st ed. Singapore: Springer Nature Singapore, 2023. pp. 1–36.

[40] Falcke H, Melia F, Agol E. Viewing the shadow of the black hole at the Galactic Center. *Astrophys. J.* 1999, 528(1):L13–L16.

[41] Doeleman SS, Weintroub J, Rogers AEE, Plambeck R, Freund R, *et al*. Event-horizon-scale structure in the supermassive black hole candidate at the Galactic Center. *Nature* 2008, 455(7209):78–80.

[42] Event Horizon Telescope Collaboration. First M87 event horizon telescope results. I. The shadow of the supermassive black hole. *Astrophys. J. Lett.* 2019, 875:L1.

[43] Event Horizon Telescope Collaboration. First Sagittarius A* event horizon telescope results. I. The shadow of the supermassive black hole in the center of the Milky Way. *Astrophys. J. Lett.* 2022, 930(2):L12–LF17.

[44] The Event Horizon Telescope Collaboration. First M87* event horizon telescope results. VII. Polarization of the ring. *Astrophys. J. Lett.* 2021, 910(1):L12.

[45] The Event Horizon Telescope Collaboration. First M87* event horizon telescope results. VIII. Magnetic field structure near the event horizon. *Astrophys. J. Lett.* 2021, 910(1):L13.

[46] The Event Horizon Telescope Collaboration. First Sagittarius A* event horizon telescope results. VII. Polarization of the ring. *Astrophys. J. Lett.* 2024, 964:L25.

[47] Zakharov AF. Shadow in the Galactic center: theoretical concept–prediction–realization. *arXiv* 2025, arXiv:2506.16927.

[48] Bambi C, Freese R. Apparent shape of super-spinning black holes. *Phys. Rev. D.* 2009, 79(4):043002.

[49] Harada T, Takahashi R. Black hole candidates and the Kerr bound. *J. Phys.: Conf. Ser.* 2011, 314(1):012084.

[50] Bambi C, Yoshida N. Shape and position of the shadow in the $\delta = 2$ Tomimatsu–Sato spacetim. *Classical Quantum Gravity* 2010, 27(20):205006.

[51] Johannsen T, Psaltis D. Testing the no-hair theorem with observations in the electromagnetic specrum. II. Black hole images. *Astrophys. J.* 2010, 718(1):446–454.

[52] Mizuno Y, Younsi Z, Fromm CM, Porth O, De Laurentis M, *et al*. The current ability to test theories of gravity with black hole shadows. *Nature Astron.* 2018, 2(7):585–590.

[53] Younsi Z, Wu K, Fuerst SV. General relativistic radiative transfer: formulation and emission from structured tori around black holes. *Astron. Astrophys.* 2012, 545:A13.

[54] Chan CK, Psaltis D, Oezel F, Narayan R, Sadowski A. The power of imaging: constraining the plasma properties of GRMHD simulations using EHT observations of Sgr A*. *Astrophys. J.* 2015, 799(1):1.

[55] Rezzolla L, Zhidenko A. New parametrization for spherically symmetric black holes in metric theories of gravity. *Phys. Rev. D,* 2014, 90(8):084009.

[56] Garca A, Galtsov D, Kechkin O. Class of stationary axisymmetric solutions of the Einstein-Maxwell-dilaton-axion field equations. *Phys. Rev. Lett.* 1995, 74(8):1276–1279.

[57] Cunha PVP, Herdeiro CAR. Shadows and strong gravitational lensing: a brief review. *Gen. Rel. Grav.* 2018, 50(4):42.

[58] Dymnikova I, Kraav K. Identification of a regular black hole by its shadow. *Universe* 2019, 5(7):163.

[59] Poisson E, Israel W. Structure of the black hole nucleus. *Classical Quantum Gravity* 1988, 5(12):L201–L205.